We thank both referees for their constructive comments to which we reply below (**RC**: referee comment; **AR**: author reply).

1 Referee #1

RC: *The article, 'Global distribution of photosynthetically available radiation on the seafloor', by JeanPierre Gattuso, presents a 21-year time series of benthic PAR. The dataset is an improved version of a prior data set (Gattuso et al., 2006). The current dataset estimates benthic PAR using ocean color and bathymetry data. The time series is four times longer with improved spatial and bathymetric resolution. The article presents a unique dataset, useful for a variety of ecological studies of the benthic community and is therefore of relevance to the scientific community. The time-series does include state-of-the-art ocean color data available to the scientific community. However, the authors are requested to consider the following comments and suggestions.*
AR: Thank you very much for your constructive comments and suggestions which significantly improved the manuscript.

1.1 Major issues

RC: *Depth range in the coastal zone ranges from about 0 – 100/150 m (Fig 4). Considering satellite receives signal only from a top layer of the ocean (referring to the concept of optical depth, the depth from which satellite receives 90% of its signal) and so Kdpar obtained from satellite data represents attenuation from this top layer, kindly explain in the manuscript how PAR obtained using equation 6 is actually bottom PAR. May be provide a schematic to explain the concept.*
AR: The confusion stems from the fact that equation 6 was incomplete. The depth it refers to is the bottom depth. Equation 6 now reads:

$$PAR_B = \exp(-K_{PAR} \times z_B) \quad (1)$$

with z_B, bottom depth.

RC: *A list of symbols and abbreviations used in the article is missing. Add one if possible and maintain consistency with Gattuso et al. 2006 for ease*

of the reader. For example, Gattuso et al. 2006, used K D and the present article uses Kd.
AR: All symbols and abbreviations are defined in the text. We therefore do not think that a list of them is needed but are happy to add one if the editor wants. We agree that terms were not used in a consistent manner. We now use K_{PAR} for the attenuation coefficient for PAR, as in Gattuso et al. (2006). K_d is the accepted term for diffuse attenuation coefficient for the downward irradiance and a given wavelength.

RC: *Page 4, line 25 states spectral composition is not considered in the study. But, throughout the manuscript irradiance is used in place of PAR.*
AR: The audience of this manuscript is both optical oceanographers, biogeochemists and ecophysiologists. These communities use different terms for the same quantity. To clarify the matter and avoid any misunderstanding, the following text will be added at the very beginning of the Methods section:

> Irradiance, here downwelling irradiance, can be defined or measured at a specific wavelength or integrated within a specific spectral domain. Photosynthetically Available Radiation (PAR in mol photons m^{-2} d^{-1}) is the amount of light available for photosynthesis, that is in the 400 to 700 nm spectral range. Biogeochemists and ecophysiologists use the term irradiance for the same quantity. Both terms are used synonymously in the present paper.

RC: *Page 2, line 2: A number of references (old as well as new) are available that provide relationships between Secchi depth and attenuation.*
`https://doi.org/10.1016/S0380-1330(88)71564-6`
`https://link.springer.com/article/10.1007/s10750-012-1084-2`
`https://doi.org/10.1016/j.rse.2015.08.002`
`https://link.springer.com/article/10.1007/s10201-008-0246-4`
AR: Thank you. A citation of Lee et al. (2015) has been added.

RC: *Page 3, section 2.1: describe the Globcolor project in a sentence or two for info.*
AR: The following text has been added.

> The GlobColour project generates global ocean colour products by merging data from current and past ocean colour instruments

> (SeaWiFS, MERIS, MODIS, VIIRS and the two OLCI). Merged products are generated through a weighted average of the level-2 geophysical products (e.g., chlorophyll) from individual missions. The weights are assigned to each mission under the form of a global uncertainty value derived through validation with respect to global databases of field observations. Alternative products are also generated through the Garver-Siegel-Maritorena (GSM) model (Garver and Siegel, 1997, Maritorena et al., 2002, 2010).

RC: *The article, throughout, refers to the present study as 2019, it needs to change to 2020 or else only stick to 'present study' and avoid mentioning the year.*
AR: Thank you. This mistake is now corrected.

RC: *Figure panels need to be labelled throughout the manuscript.*
AR: Figure panels are identified in the revised version of the manuscript.

RC: *Figure 1 caption: Availability of remote sensing data (monthly mean) over the 21 years' time-series expressed on percentage. The other half of the caption regarding surface of the coastal zone is not clear and difficult to understand. Please explain in a different sentence.*
AR: The legend now reads as follows:

> Availability of remote sensing data over the 21-year time-series. Availability is expressed as the monthly mean of the percent area of each latitudinal band covered by the satellite

RC: *Page 13, Figure 5: P1 P2 P3 not explained in the caption. Y axis refers to irradiance or PAR? Units refer to PAR.*
AR: P1 to P3, which referred to time periods, are not needed and have been removed. Irradiance and PAR are used synonymously. See justification above.

RC: *Page 14, Table 3: Z surface 1% refers to depth at which benthic irradiance or benthic PAR equals 1% of surface?*
AR: Text changed accordingly.

RC: *Table 4: Could the increased PAR in the Arctic be attributed to increased* *sea ice melting? Possible to check and provide evidence if this increase is more prominent in the last decade?*

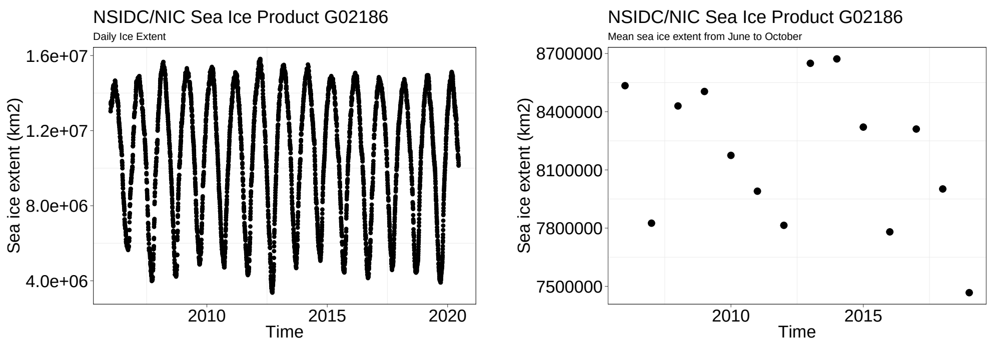

Figure 1: Sea ice extent in the Northern hemisphere.

AR: Changes in the penetration of light in the Arctic Ocean are complex to analyze and predict. The loss of sea ice favours the penetration of light but the increased input of dissolved and particulate matter in the coastal zone (the region of interest in the present paper) resulting from the melting of land ice and permafrost restricts light penetration. We had a look at data Multisensor Analyzed Sea Ice Extent - Northern Hemisphere (MASIE-NH), Version 1 (downloaded on 19 June from `https://nsidc.org/data/G02186/versions/1`; Fig. 1). There is no obvious change in the daily extent of sea ice nor in the average sea ice extent during the period of June to October (the period of interest in the present paper). A correlation between light penetration and the extent of sea ice may exist at subregional scale but investigating such relationship goes well beyond the scope of this paper. We therefore refrain from making any statement on the role of sea ice loss on benthic PAR in the Arctic.

1.2 Technical comments

RC: *Page 1, line 1: Abstract (delete the period) Page 1, line 2: global distribution of light (photosynthetically available radiation; PAR)*
AR: Is the referee referring to the semi colon? It is justified here.

RC: *Page 1, line 3: to estimate benthic irradiance or benthic PAR?*
AR: Irradiance and PAR are used synonymously. See justification above.

RC: *Page 1, line 3: avoid using references in the abstract*

AR: The citation has been removed.

RC: *Page 1, line 16: lowest levels of food web*
AR: The typo has been corrected, thanks. Web is plural because there are many distinct food webs.

RC: *Page 2, line 7: However, in the coastal ocean, primary production also occurs at the bottom, when enough light reaches the sea floor.*
AR: The text has been changed accordingly.

RC: *Page 2, line 10: in the past 10 years. (delete the period) Page 2, line 14-15: Irradiance or PAR?*
AR: Done. Irradiance and PAR are used synonymously. See justification above.

RC: *Page 2, line 19: Glud et al. ??*
AR: Missing year added.

RC: *Page 2, line 20: a data layer of benthic irradiance for modelling of species distribution as part of*
AR: The text has been changed accordingly.

RC: *Page 2, line 31: the characteristics of products used by Gattuso et al. (2006) and of those in the present study*
AR: The text has been changed accordingly.

RC: *Page 3, line 1: Table 1. Main characteristics of the products used in Gattuso et al. (2006) and of those in the present study.*
AR: The text has been changed accordingly.

RC: *Page 3, line 21: at level-2 of the processing Page 4, line 7: It was carried out Page 4, line 13: (Morel and Belanger, 2006) Page 4, line 21: Benthic Irradiance or Benthic PAR?*
AR: Correction made. Irradiance and PAR are used synonymously. See justification above.

RC: *Page 4, equations 2, 3: explain each of the terms Page 7, table 2 caption: Values reported in Gattuso et al. (2006) are shown in parentheses for comparison.*

AR: Every term is now defined. Change in the caption done.

RC: *Page 7, line 14: The surface area of the ocean with depth less than 200*
AR: Done.

RC: *Page 7, line 16: the Antarctic (60 to 90S) regions, respectively covering 24.1, 75.5, and 0.6% surface area of the global coastal zone.*
AR: Done.

RC: *Page 8, line 4: In the Arctic and the Antarctic, sunlight is available only during the 5 summer months of the year, i.e., June to October and November to March respectively.*
AR: Done.

RC: *Page 8, line 5: Furthermore, data availability is higher in mid-summer than in . . . .*
AR: Done.

RC: *Page 8, line 12-13: In contrast, there is a clear dominance of Case 1 over Case 2 waters (70 vs 30%) in the non-polar region whereas it was more even (55 vs 45%) in Gattuso et al. 2006.*
AR: Done.

RC: *Page 8, line 15: The present study uses remote. . .*
AR: Done.

RC: *Page 9, line 10: The distribution of PAR B has changed in the present study compared to Gattuso et al. (2006), ...*
AR: Done.

RC: *Page 9, Figure 2 caption, delete 2019*
AR: Done.

RC: *Page 10, Figure 3: left and the right panel not mentioned in the caption. Y axis in the right panel refers to 2019? check the axis title*
AR: The figure and legend have been corrected accordingly.

RC: *Page 11, Figure 4: left and the right panel not mentioned in the caption*
AR: Now they are.

RC: *Page 11, line 4: As shown in fig. 3, In the non-polar region, higher the irradiance threshold, larger the difference.*
AR: Text modified accordingly.

2 Referee #2

RC: *This manuscript should be accepted for publication pending some editing. The science appears to be sound and results are potentially very useful to a wide range of readers, as the authors note in the Introduction and Conclusions. The role of light in biogeochemical cycles, especially the carbon cycle, is so fundamental that many researchers overlook the important details, such as those presented in this paper. My comments are primarily editorial, with the goal of making the manuscript a bit easier to read.*
AR: Thank you very much for your constructive comments and suggestions.

RC: *One common challenge for the reader is the authors' frequent use of ambiguous pronouns. For example, starting a sentence wit"I", when the closest singular noun is not what the authors are referring to (e.g., second line of the Abstract and also in the Conclusions). Even more nebulous is beginning paragraphs with "It is. . ." when rearranging the topic sentence slightly can provide clarity.*
AR: We believe this issue has been addressed in the revised version of the manuscript.

RC3: *Inconsistencies are persistent throughout the manuscript, including in the figures and tables. For example, the authors use non polar, non-polar, Non polar, Non-polar, Non-Polar, and even NonPolar. Many of those usages are highlighted in the manuscript pdf that is annotated with comments (provided).*
AR: We agree and now use nonpolar, which is a correct English term, throughout the manuscript.

RC: *Related to this issue is the placement of "Arctic" and "Non pola" graphs in the figures. In Figure 2, Arctic is on the left, but on the right in figures 3 and 4. Similarly, there is no consistency to heading placement in the tables. Also, in Table 5, please provide units for Irradiance. Are the authors referring to mol photons m-2 d-2 or to percent of surface irradiance.*
AR: We agree. Now the regions are shown in the same order in all tables

and figures: Arctic, nonpolar and Antarctic. The unit of irradiance is now provided in Table 5.

RC: *Another ambiguity for the reader is the sparse use of "benthic" when referring to photosynthetic organisms in the "Results and discussio". This ambiguity is particularly problematic when referring to "surface area", which generally appears to refer to surface area of the ocean, though the Figure 3 caption does refer to the "surface area of the sea floo". The authors could revise their wording to clarify for the reader, especially in section 3.4, when they are specifically referring to benthic photosynthesis, productivity, communities, etc.*
AR: Comment addressed in the revised version of the manuscript.

Global distribution of photosynthetically available radiation on the seafloor

Jean-Pierre Gattuso[1,2], Bernard Gentili[1], David Antoine[1,3], and David Doxaran[1]

[1]Sorbonne Université, CNRS, Laboratoire d'Océanographie de Villefranche, 181 chemin du Lazaret, F-06230 Villefranche-sur-mer, France

[2]Institute for Sustainable Development and International Relations, Sciences Po, 27 rue Saint Guillaume, F-75007 Paris, France

[3]Remote Sensing and Satellite Research Group, Curtin University, Perth, Western Australia, 6845, Australia

Correspondence: J.-P. Gattuso (gattuso@obs-vlfr.fr)

Abstract.

A 21-year (1998–2018) continuous monthly data set of the global distribution of light (~~photosynthetically available radiation;~~ Photosynthetically Available Radiation, PAR, or irradiance) reaching the seabed is presented. ~~It~~ This product uses ocean colour and bathymetric data to estimate benthic irradiance, offering critical improvements on a previous data set~~(Gattuso et al., 2006)~~. The time series is 4 times longer (21 vs 5 years), the spatial resolution is better (pixel size of 4.6 vs 9.3 km at the equator) and the bathymetric resolution is also better (pixel size of 0.46 vs 3.7 km at the equator). The paper describes the theoretical and methodological bases and data processing. This new product is used to estimate the surface area of the sea floor where (1) light does not limit the distribution of photosynthetic benthic organisms and (2) net community production is positive. The complete data set is provided as 14 netCDF files available on PANGAEA (Gentili and Gattuso, 2020, https://doi.pangaea.de/10.1594/PANGAEA.910898). The R package CoastalLight, available on Github (https://github.com/jpgattuso/CoastalLight.git), allows (1) to download geographical and optical data from PANGAEA and (2) to calculate the surface area that receives more than a given threshold of irradiance in three regions (non polar, Arctic and Antarctic). Such surface areas can also be calculated for any sub-region after downloading data from a remotely and freely accessible server.

1 Introduction

Light is a key ocean variable. It shapes the composition of benthic and pelagic communities by controlling the three-dimensional distribution of primary producers, the lowest levels of the ~~wood~~ food webs. Light also plays a major role in the global carbon cycle by controlling primary production, the main source of new organic carbon in the ocean (Assis et al., 2018). In the marine environment, sunlight is rapidly absorbed by the water column and primary production is restricted to the shallow photic zone above 200 m depth (except for localized chemo-autotrophic communities). Marine diazotrophs, which fix dinitrogen into organic forms, are also light-dependent. Furthermore, many marine ecosystem engineers require light because they are either plants (mangrove, saltmarshes, seagrass, coralline algae) or animals living in symbiosis with endosymbiotic algae (e.g., some molluscs and zooxanthellate, reef-building corals).

Until the late 1970s, most water transparency measurements were performed using Secchi disks (Tyler, 1968) and several formulations became available to convert Secchi disk readings to attenuation coefficients (e.g., Weinberg, 1976)(e.g., Weinberg, 1976; Lee et . Remote sensing observations of ocean colour showed great promise as early as 1978, when the Coastal Zone Color Scanner (CZCS) was launched. It was followed by several other instruments on-board satellites. Ocean colour measurements of the Sea-Viewing Wide Field-of-View Sensor (SeaWiFS), launched in 1997, are used to derive the concentration of chlorophyll-a (C_{sat}) and the mean attenuation coefficient for PAR (K_{PAR}). Until 2006, most attention was focused on the light field in the water column to derive open-ocean primary production (e.g., Antoine et al., 1996). However, in the coastal ocean, primary production also occurs in the coastal ocean at the bottom, when enough light reaches the sea floor. For example, on coral reefs, benthic primary production can represent 90% of the total primary production (Delesalle et al., 1993). Primary production in coastal vegetated habitats such as mangroves, seagrass beds and tidal marshes, the so-called 'blue carbon ecosystems', has received considerable interest in the past 10 years , because of their disproportionately large contribution to global carbon sequestration (Macreadie, 2019). It has been recently suggested that benthic macroalgae also contribute to global carbon burial (Krause-Jensen et al., 2018).

Gattuso et al. (2006) used SeaWiFS data collected between 1998 and 2003 to estimate, for the first time at a nearly global scale, the irradiance reaching the bottom of the coastal ocean. They provided cumulative functions to estimate the percentage of the surface area (S) of the coastal zone receiving more than a given irradiance. These data were used to investigate the extent of macroalgae (Krause-Jensen and Duarte, 2016), restoration of seagrass ecosystems (Eriander, 2017), role of vegetated coastal habitats in the ocean carbon budget (Duarte, 2017), macroalgal subsidies supporting benthic invertebrates (Filbee-Dexter and Scheibling, 2015), global continental shelf denitrification (Eyre et al., 2013), and benthic primary production in the Arctic Ocean (Attard et al., 2016; Glud et al., 2009).

More recently, Assis et al. (2018) provided a data layer for of benthic irradiance for species distribution modelling modelling of species distribution as part of the Bio-ORACLE set of GIS rasters. This data set is based on $K_{d,490}$ $K_d(490)$ in contrast to Gattuso et al. (2006) who used the more appropriate K_{PAR} to estimate bottom PAR (PAR_B). This is particularly important in coastal regions where there is no unique relationship between $K_{d,490}$ $K_d(490)$ and K_{PAR} due to large differences in the concentration and composition of non-algal coloured substances.

Since these first efforts, new products have become available which can improve estimates of the global distribution of benthic irradiance. These include a much longer time series of ocean colour (21 vs 5 years) with an improved spatial resolution (4.6 vs 9.3 km at the equator). Bathymetric data have also considerably improved since 2006 (0.46 vs 3.7 km at the equator). Here we make use of these new products to provide a global distribution of photosynthetically available radiation reaching the seafloor.

2 Methods

Irradiance, here downwelling irradiance, can be defined or measured at a specific wavelength or integrated within a specific spectral domain. Photosynthetically Available Radiation (PAR in $\mathrm{mol\ photons\ m^{-2}\ d^{-1}}$) is the amount of light available for photosynthesis, that is in the 400 to 700 nm spectral range. Biogeochemists and ecophysiologists use the term irradiance for the same quantity. Both terms are used synonymously in the present paper. The characteristics of the products used by Gattuso et al. (2006) and of those in the present study are compared in Table 1 .

Table 1. Main characteristics of the products used by Gattuso et al. (2006) and of those in the present study.

	Gattuso et al. (2006)	Present study
Satellite	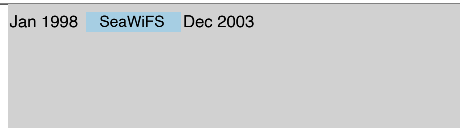	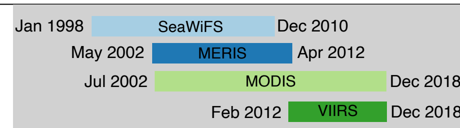
Coverage	1998 to 2003	1998 to 2018
Sat. resolution	$\approx 1/12°$ = 9.3 km at equator	$\approx 1/24°$ = 4.6 km at equator
Bathymetry	ETOPO 2 min	GEBCO 15 sec
	3.7 km at equator	0.46 km at equator
Data	PAR, C_{sat}, $nLw(555)$, ~~K_d~~ K_{PAR} from C_{sat}	PAR, K_{PAR}, C_{sat}, $R_{rs}(555)$

2.1 Remote sensing data

Monthly ~~Level-3~~ level-3 data of PAR (mol photons m^{-2} d^{-1}), K_{PAR} (m^{-1}), concentration of chlorophyll-a (C_{sat}, mg m^{-3}), and remote sensing reflectance at 555 nm ($R_{rs}(555)$, sr^{-1}) from the ~~four~~ satellite-borne sensors SeaWiFS, Moderate Resolution Imaging Spectroradiometer (MODIS), MEdium Resolution Imaging Spectrometer (MERIS) and Visible Infrared Imaging Radiometer Suite (VIIRS) were obtained from the GlobColour project (http://www.globcolour.info). The GlobColour project generates global ocean colour products by merging data from current and past ocean colour instruments (SeaWiFS, MERIS, MODIS, VIIRS and the two OLCI) but data retrieved from GlobColour in January 2019 did not comprise data from the Ocean and Land Colour Imager (OLCI). Merged products are generated through a weighted average of the level-2 geophysical products (e.g., chlorophyll) from individual missions. The weights are assigned to each mission under the form of a global uncertainty value derived through validation with respect to global databases of field observations. Alternative products are also generated through the Garver-Siegel-Maritorena (GSM) model (Garver and Siegel, 1997; Maritorena et al., 2002, 2010) . The resolution is 1/24°. Together, the 252 monthly images downloaded (a level-3 image contains values of a product on a regular longitude-latitude grid) cover the period 1998 to 2018.

2.2 Bathymetry and coastline

Depths were estimated from the 2019 General Bathymetric Chart of the Oceans (GEBCO; https://www.gebco.net) gridded bathymetry data (1/240°resolution). The coastal zone (0 to 200 m) was determined using a land mask and coastline (Global Self-consistent, Hierarchical, High-resolution Geography, GSHHG) as implemented in the Generic Mapping Tools (GMT;

Wessel et al., 2013). The full resolution was used. The Arctic, Antarctic, and non polar regions represent, respectively, 24.1, 0.6, and 75.3% of the surface area of the coastal zone.

2.3 Case 1 versus Case 2 waters

It is beyond the scope of this paper to review the criteria used to eliminate dubious data when generating a Level-3 level-3 ocean colour composite, except for discriminating the water type as being either Case 1 or Case 2 (Morel and Prieur, 1977). In Case 1 waters, where phytoplankton and associated degradation products are the main contributors to light attenuation (but see Claustre and Maritorena, 2003), K_{PAR} can be modelled as a function of the concentration of chlorophyll-a, itself derived from reflectance values. The situation is, however, not as straightforward in Case 2 coastal waters where light attenuation by coloured dissolved organic matter and suspended particles other than phytoplankton can be significant and not correlated to the chlorophyll-a concentration. The discrimination between these two types is performed at the Level-2 in level-2 of the processing, yet it is not considered when generating the Level-3 level-3 composites (B. Franz, personal communication, September 2019). Therefore, the average chlorophyll-a concentration C_{sat} in a given bin of a Level-3 level-3 composite may have been computed over any proportion of Case 1 and Case 2 waters.

The accuracy of C_{sat} in Case 1 waters is claimed to be ±30% whereas it is unknown in Case 2 waters. It is therefore not possible to estimate the accuracy of the chlorophyll product in coastal areas and, in turn, the accuracy of the diffuse attenuation coefficient. The determination of the water type could not be performed with specific algorithms for each water type since no universal algorithm exists for Case 2 waters. It was was carried out *a posteriori* based on the average C_{sat} and $R_{rs}(555)$. This determination provides an indication of bins that likely belong to the Case 2 water category when, on average, the individual pixels accumulated in the bins were predominantly of the Case 2 type.

The identification of turbid Case 2 waters has been performed as in Morel and Bélanger (2006) by comparing the water reflectance at 555 nm ($R(555)$) to the maximum value it should have in Case 1 waters and for the same chlorophyll concentration ($R_{lim}(555)$). Note that the water type was set to Case 1 for any pixel where $C_{sat} < 0.2$ mg m^{-3}, because the algorithm is occasionally subject to falsely classify low-chlorophyll waters as Case 2 Morel and Bélanger (2006)(Morel and Bélanger, 2006) . Turbid Case 2 waters are those for which $R(555) > R_{lim}(555)$. To perform this test, $R_{rs}(555)$ was converted to $R(555)$ as follows (Morel and Gentili, 1996):

$$R(555) = R_{rs}(555) \times Q_0(555)/\Re_0 \tag{1}$$

where $Q_0(555)$ is the chlorophyll-dependent Q-factor (sr), i.e., the ratio of the upward irradiance to the upwelling radiance (Morel et al., 2002), and $\Re_0$ is a term that merges all reflection and refraction effects at the air-sea interface (on average equal to 0.529). Since $R_{rs}(555)$ is fully normalized (Morel and Gentili, 1996), its dependence on the viewing angle and the sun zenith angle are removed so that both Q and $\Re$ are taken for a nadir view and a sun at zenith (hence the "0" subscript).

2.4 Benthic irradiance

The $K_d(\lambda_0, z)$, the diffuse attenuation coefficient for the downward irradiance $K_d(\lambda_0)$ (E_d) for a given wavelength λ_0, describes the exponential attenuation of irradiance with depth in the water column. It determines the amount of radiation reaching any given depth a given depth (z):

$$K_d(\lambda_0, z) = \frac{-\partial \ln(E_d(\lambda_0, z))}{\partial z} \tag{2}$$

The spectral composition of the radiation is not considered in this work and only its integral value between 400 and 700 nm is used (i.e., the photosynthetically available radiation, PAR). The attenuation coefficient for PAR is therefore:

$$K_{PAR}(z) = \frac{-d\ln(PAR(z))}{dz} \tag{3}$$

The average value K_{PAR} of $K_{PAR}(z)$ over the euphotic zone, approximated as the depth where PAR is reduced to 1% of its value just beneath the sea surface, is computed from the corresponding chlorophyll concentration for Case 1 waters C_{sat} and $K_d(490)$ using the following equations (Morel et al., 2007; ACRI-ST GlobColour Team, 2017) :

$$K_d(490) = 0.0166 + 0.08349 \times C_{sat}^{0.63303} \tag{4}$$

$$K_{PAR} = 0.0665 + 0.874 \times K_d(490) - 0.00121/K_d(490) \tag{5}$$

The bottom irradiance irradiance at the bottom depth (z_B) is then calculated:

$$PAR_B = \exp(-K_{PAR} \times z_B) \tag{6}$$

- for the Non-Polar region all months are taken into account, so we have 21 years $\times$ 12 months = 252 values by pixel at most
- for the Arctic region months 6-10 (June to October) are taken into account, so we have 21 years $\times$ 5 months = 105 values by pixel at most
- for the Antarctic region months 1-3 and 11-12 (January to March and November-December) are taken into account, so we have 21 years $\times$ 5 months = 105 values by pixel at most
- in fine, we have 252 monthly PAR_B images for the non polar region and 105 for the Arctic and Antarctic regions.

The product delivered comprises longitude, latitude, depth, area, PAR, K_{PAR}, PAR_B for each coastal pixel. PAR, K_{PAR} and PAR_B are monthly climatologies or a climatology over the entire time series (see Section 4). The calculation of surface area receiving PAR_B above a certain threshold does not use these climatologies.

2.5 Surface area receiving light above a certain threshold

Calculations of surface area receiving PAR_B above a certain threshold are made in two steps. First a $\mathcal{P}$-function is calculated with the available pixels; then the area is calculated as the product of the $\mathcal{P}$-function by the surface of the coastal zone (0-200 m).

2.5.1 The three main regions

A region is defined here by an interval of latitude at the surface of the Earth. Polar regions are more frequently observed by satellites, yet polar night and cloudiness end up with data not being available several months a year. So three regions have been defined:

- the "non polar" region $[60°\text{S}; 60°\text{N}]$, where data are always available,
- the "Arctic" region $[60°\text{N}; 90°\text{N}]$, where data are available during the months of June, July, August, September, and October,
- the "Antarctic" region $[90°\text{S}; 60°\text{S}]$, where data are available during the months of January, February, March, November, and December.

2.5.2 $\mathcal{P}$-functions

Definition of a $\mathcal{P}$-function for a monthly PAR_B image of a region

- let I be the monthly image (values of PAR_B on the floor of the coastal zone of the region)
- let $S_{a,I}$ be the available surface, i.e. the total surface of pixels for which an irradiance value is available (varying every month);
- let E a value of irradiance (expressed in $\text{mol photons m}^{-2}\text{ d}^{-1}$);
- let $s_I(E)$ the total surface of pixels collecting irradiance greater than E;
- the $\mathcal{P}_I$-function if defined as $\mathcal{P}_I(E) = 100 s_I(E)/S_{a,I}$

Definition of a climatologic $\mathcal{P}$-function

Our purpose is now to define a $\mathcal{P}$-function for a set of monthly values $\mathcal{I} = \{I_i, i = 1 \dots n\}$. Giving a value of irradiance E, it is defined as :

$$\mathcal{P}_{\mathcal{I}}(E) = 100 \sum_{i=1}^{n} s_{I_i}(E) / \sum_{i=1}^{n} S_{a,I_i} \tag{7}$$

Climatologic monthly $\mathcal{P}$-function

In this case, the 21 data sets available for a given month through the entire time-series (1998 to 2018) are selected to calculate the $\mathcal{P}$-function according to equation 7. So we have :

- 12 climatologic monthly $\mathcal{P}$-functions for the Non-Polar region,
- 5 climatologic monthly $\mathcal{P}$-functions for the Arctic region,
- 5 climatologic monthly $\mathcal{P}$-functions for the Antarctic region.

Climatologic global $\mathcal{P}$-function

$\mathcal{P}_g$ is obtained, using all data sets (252 for Non-Polar and 105 for Arctic and Antarctic) in equation 7.

$\mathcal{P}$-functions for a subregion

Sub-region may be defined within one of the three main regions. In this case data sets are clipped according to the sub-region's boundaries, and the months used are those of the main region. Calculation is identical to that described above for the climatological global $\mathcal{P}$-function (section 2.5.2). The R package *CoastalLight* (see Section 4) can be used to calculate a $\mathcal{P}$ function for a subregion with the help of a remote server.

2.5.3 Surface areas

Let $\mathcal{P}$ be the $\mathcal{P}$-function of the zone and S_{geo} its area : the area receiving irradiance above a threshold E is :

$$s(E) = S_{geo}\,\frac{\mathcal{P}(E)}{100} \tag{8}$$

3 Results and discussion

The present study essentially confirms the bathymetric data reported in our earlier study (Gattuso et al., 2006) but shows substantial differences on the optical data.

3.1 Surface area and depth of sub-regions of the ocean

The area and depth of the three regions measured with the most recent GEBCO bathymetry are very similar to those obtained with the coarser ETOPO2 data set used by Gattuso et al. (2006) (Table ??2). The surface area of the ocean with depth less than 200 m depth is 25.3 10^6 km^2. Three geographical areas are considered: the Arctic (60 to 90°N), non polar the non polar region (60°N to 60°S), and the Antarctic (60 to 90°S) regions, respectively covering 24.1, 75.5 and 0.6% of the global coastal zone. The average depth of the coastal zone is almost twice as large in the Antarctic than in the Arctic and non polar nonpolar regions (137 vs 77 and 71 m).

Table 2. Surface area (S) of coastal waters (depth < 200 m) of different optical characteristics. Calculations were performed on monthly products. Values reported by Gattuso et al. (2006) are shown in parentheses for ~~comparative purposes~~comparison. Gattuso et al. (2006) did not report data for the Antarctic.

	Arctic		Nonpolar		Antarctic	
	~~$S(10^6 km^2$~~$S(10^6$ km$^2)$	$S(\%)$	~~$S(10^6 km^2$~~$S(10^6$ km$^2)$	$S(\%)$	~~$S(10^6 km^2$~~$S(10^6$ km$^2)$	$S(\%)$
Coastal Zone	6.1 (6.13)	100 (100)	~~0.146100~~19.1 (18.8)	100 (100)	0.146	100
Case 1	2.37 (1.6)	38.8 (26.2)	~~0.02920.1~~11.3 (8.47)	59.2 (45)	0.029	20.1
Case 2	0.72 (0.81)	11.8 (13.2)	~~0.02214.8~~4.62 (6.76)	24.2 (35.9)	0.022	14.8
Case 1 and Case 2	3.08 (2.41)	50.5 (39.40)	~~0.05134.9~~15.9 (15.23)	83.4 (80.9)	0.051	34.9

3.2 Availability of ocean colour data and seawater types

The availability of monthly ocean colour data is highly variable depending on the latitude and month of the year (Fig. 1). It is highest in ~~non polar~~ nonpolar regions where, on average, data are available in 83% (range: 62-96%) of the pixels in monthly data sets. ~~There is light for only~~ In the Arctic and the Antarctic, sunlight is available only during the 5 summer months of the year~~in the Arctic (~~, i.e., June to October ~~) and Antarctic (~~and November to March~~). During these periods~~, respectively. Furthermore, data availability is higher in mid-summer than in early- and late summer (Fig. 1). Data availability also decreases as one gets closer to the poles. On average, data are available for 51 and 35% of the summer data sets in the Arctic and Antarctic regions (ranges: 6-89% and 11-58%, respectively; ~~??). It~~ Table 3). Data availability is higher in the present study which used multiple sensors than in a previous study that only used SeaWiFS data (Gattuso et al., 2006). Several factors contribute to the lower availability of data in polar regions: pixels are contaminated by sea ice and flagged accordingly, high occurrence of cloudy days and low incidence of the sun.

The coverage of the Arctic has improved with about 20% more pixels with available data (Table ~~??~~3). Case 1 and Case 2 waters are approximately equally distributed in the Antarctic region (Table ~~??~~2). In contrast, ~~the distribution of Case 1 and Case 2 waters in the non polar region, with~~ there is a clear dominance of Case 1 over Case 2 waters (70 vs 30%) in the ~~present study~~ nonpolar region whereas it was more even (55 vs 45%) in Gattuso et al. (2006, 55 vs 45%). This difference may be due to the different approaches used to differentiate Case 1 and Case 2 waters. The present study ~~used~~ uses the remote sensing reflectance at 555 nm ($R_{rs}(555)$) provided by the GlobColour project whereas it was roughly estimated from the normalized water-leaving radiance in the previous study (Eq. 1 in Gattuso et al., 2006). The quality of the results should therefore have improved. In any case, the usefulness of this distinction is relatively limited because the light penetration through the water column is calculated in the same way in the two cases. The distribution of water quality is however useful to estimate the reliability of the bottom irradiance which is much better in Case 1 waters than in Case 2 waters. The average depth of the missing pixels is similar to that of the available pixels in the Arctic and Antarctic regions (Table 3). However, it is sometimes lower in the ~~non polar~~ nonpolar region. The lowest values occur when the amount of available pixels is the largest (data not shown), suggesting that the missing pixels are preferentially located close to the coastline.

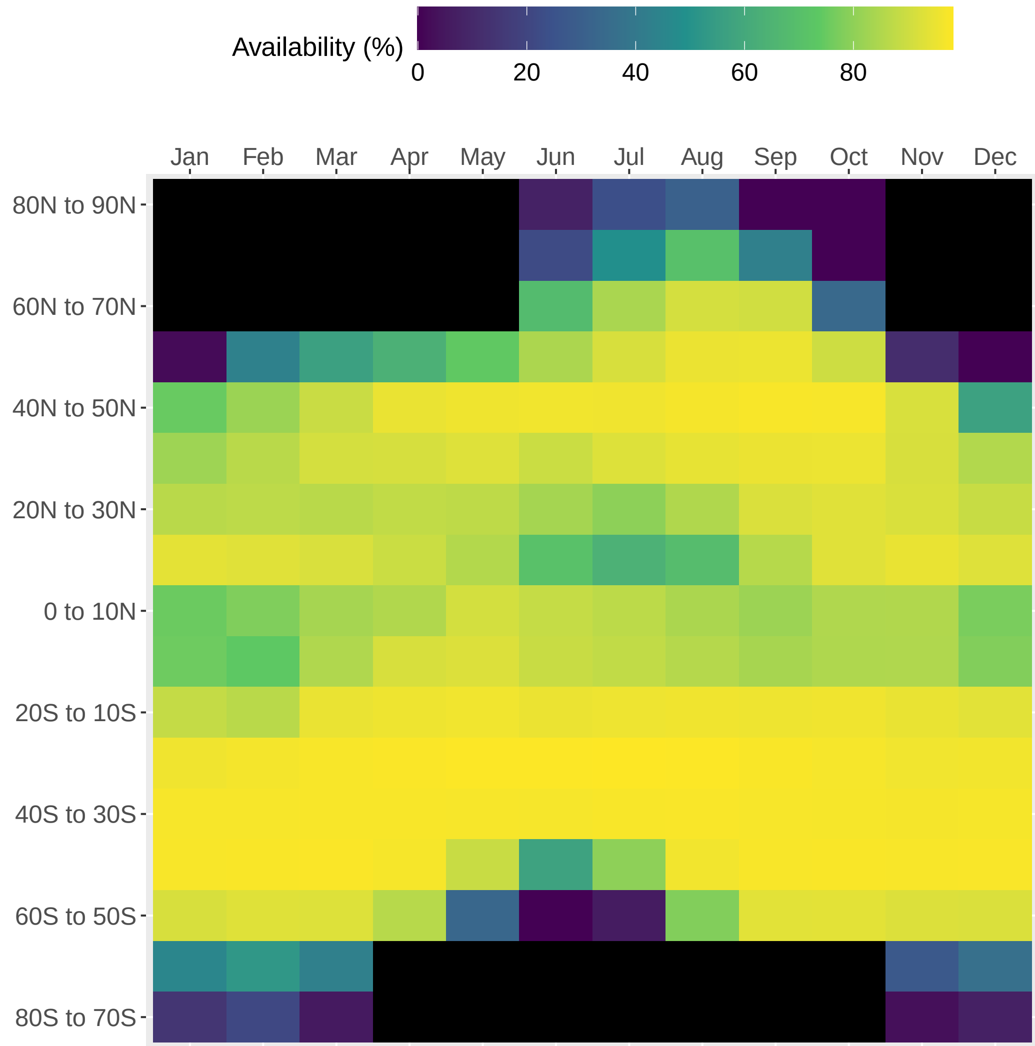

Figure 1. ~~Mean monthly availability~~ Availability of remote sensing data over the ~~entire 21 years~~ 21-year time-series. Availability is expressed as the ~~percent~~ monthly mean of the ~~surface~~ percent area of ~~the coastal zone in~~ each latitudinal band covered by the satellite.

3.3 Bottom irradiance

The distribution of ~~PAR_B~~ PAR_B has changed in the present study compared to ~~the previous one of~~ Gattuso et al. (2006), with less irradiance values above 0.2 $\mathrm{mol\ photons\ m^{-2}\ d^{-1}}$ and more irradiance values around 0.1 $\mathrm{mol\ photons\ m^{-2}\ d^{-1}}$ in ~~2019~~ the present study than in 2006 (Fig. 2).~~Consequently, the surface area receiving irradiance above a certain threshold also declined (Fig. 3).~~

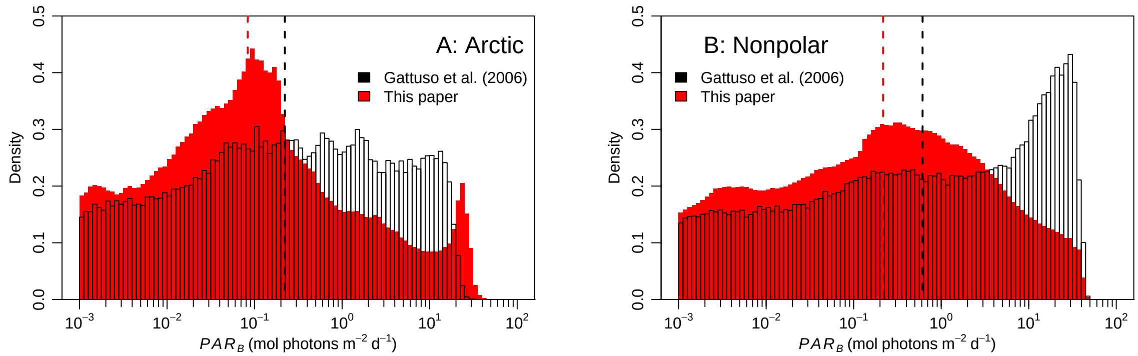

Figure 2. Distribution of PAR_B in the ~~present study~~ Arctic (~~2019~~A) and nonpolar (B) regions in the present study and in Gattuso et al. (2006). The vertical dashed lines represent the median values in ~~2006~~ Gattuso et al. (2006) (black) and the present (red) studies.

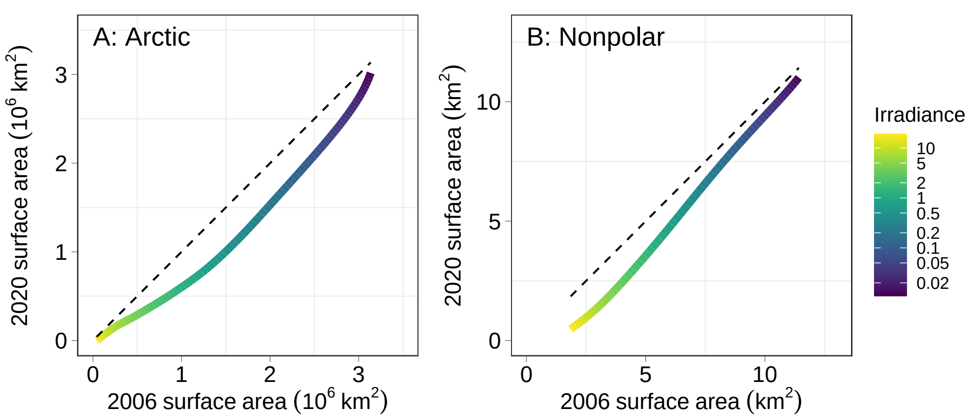

Figure 3. Comparison of the surface area of the sea floor of the Arctic (A) and nonpolar (B) regions receiving an irradiance larger than a threshold value ranging from 0.01 to 20 $\mathrm{mol\ photons\ m^{-2}\ d^{-1}}$ calculated in the present paper (2020) compared with the surface area reported ~~in 2006~~ by Gattuso et al. (2006). The dotted line is the 1:1 relationship.

The surface area of the sea floor receiving an irradiance larger than a threshold value is lower than with the previous estimate of Gattuso et al. (2006)(Fig. 3). Differences are low below an irradiance threshold of 0.2 $\mathrm{mol\ photons\ m^{-2}\ d^{-1}}$: 3 to 16% lower, respectively in the ~~non polar~~ nonpolar and Arctic regions. However, differences are as high as 26 and 56%, respectively in the non polar nonpolar and Arctic regions for irradiance thresholds ranging between 10 and 50 $\mathrm{mol\ photons\ m^{-2}\ d^{-1}}$. Such differences can be due to several causes.

The present study and Gattuso et al. (2006) used different approaches. In the 2006 study, a p-function $\mathcal{P}$-function was derived for each month and then monthly means calculated, implicitly giving the same weight to each month, irrespective of the number of pixels with available data. In the present study, each month has a weight proportional to the surface area for which data are available, hence providing better estimates. Second, there are more data available in the data set compiled in the present paper, especially in the Arctic. Third, Gattuso et al. (2006) fitted polynomial functions on the relationship between irradiance and the cumulative surface area of the sea floor receiving irradiance above a prescribed threshold. These functions only provide rough estimates and are not used in the present study. They are shown for comparative purposes in Fig. A1. The R package CoastalLight has been developed in the present study to provide more accurate estimates (Section 4) calculated from the underlying data, that is the number of pixels and their size.

These changes in approach, together with the different data sets used for the optical and bathymetric data, have led to significant changes in three factors that affect bottom PAR (PAR_B, Fig. 4, Table 4). Two of them contribute to a decline of bottom PAR PAR_B: (1) a change in the depth distribution leading to an increase in the median depth (39 vs 31 m) and (2) the a distribution of K_{PAR} moved towards larger values in 2019. that moved towards higher values in the present study. Also, (3) surface PAR , which controls PAR_B, tends to be higher in the present study than in the previous one. We do not have any independent confirmation of such an increase in surface PAR globally. The change could be real but could also result from successive reprocessing of the individual sensor archives that made up the GlobColour products that have occurred since 2006. These reprocessing indeed include updates of calibration coefficients and possible refinements of algorithms. The combined effects of the first two causes are larger that the effect of the third one, explaining why bottom PAR is overall smaller in the present study than in the previous one (Gattuso et al., 2006).

Median values of the products used by Gattuso et al. (2006) and the present study.Gattuso et al. (2006)Present study Non polar 42.5 45Arctic 31.4 38.5Non polar 0.0968 0.1336Arctic 0.1407 0.1630Non polar 41 41Arctic 19 22

3.4 Implications for the distribution of photosynthetic organisms and communities

The differences in PAR_B between the 2006 study and the present one have implications on the potential surface areas receiving enough irradiance to sustain growth of photosynthetic organisms and communities (Table 5). Surface areas are 4 to 47% lower in the present study depending on the region and organism or community considered. As shown in Fig. 3, in the non polar regionnonpolar region, the higher the highest the irradiance threshold, the largest the larger the difference. Hence, the differences are generally reasonable (less than 15%) for organisms but higher (up to 47%) for communities which have higher light requirements to maintain positive rates of net primary production. Differences between the 2006 estimates and the present ones are generally larger in the Arctic than in the non polar nonpolar region for organisms and fairly similar for communities.

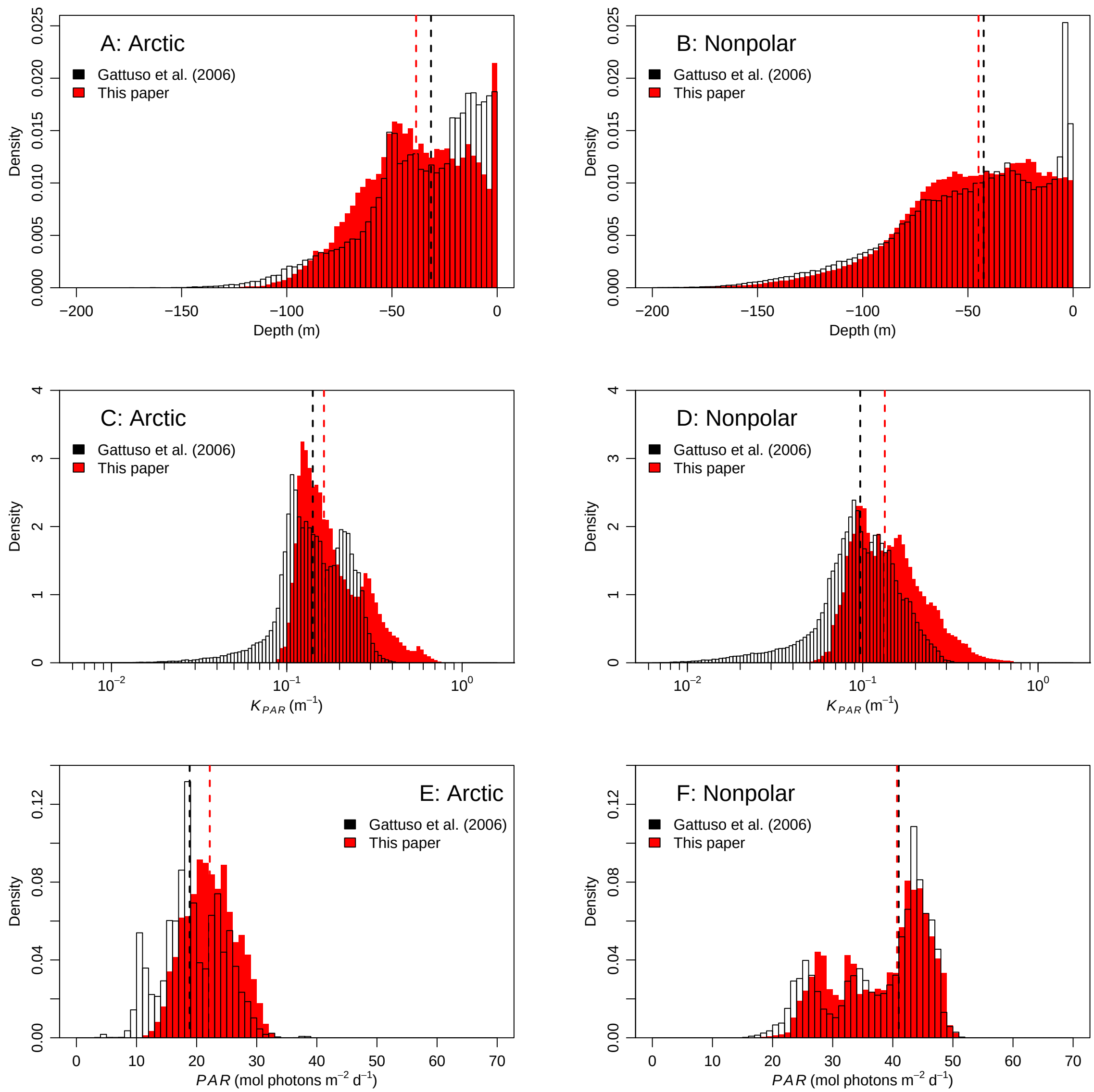

Figure 4. Distribution of depth, K_{PAR} and ~~PAR~~ PAR in the present study and in Gattuso et al. (2006). The vertical dashed lines represent the median values in the 2006 (black) and present (red) studies.

3.5 Analysis of time series

Long-term changes in the optical characteristics have recently been described. For example, using SeaWiFS monthly global ocean transparency data over Sep. 1997 to Nov. 2010, He et al. (2017) described a rapid decrease in global mean ocean transparency at a rate of -0.85 m yr^{-1} between 1997 and 1999, followed by a small increase with a rate of 0.04 m yr^{-1} over 2000–2010.

In the Arctic coastal zone, significant climate change effects have been observed over the last two decades including enhanced melting of sea-ice during the summer period, permafrost thaw and increase of river discharge into the Arctic Ocean. Time-series of ocean color satellite data have been successfully used to confirm these changes and quantify an increase of up to 40% in the concentrations of both dissolved and particulate terrestrial substances in Arctic coastal waters (Doxaran et al., 2015, Matusoka, pers. comm.). In ~~non polar~~ nonpolar regions, satellite observations did not reveal such significant temporal trend (e.g., Loisel et al., 2014) but often highlighted how human-induced activities impact on the discharge of big rivers and its consequences on the turbidity of surrounding coastal waters (Feng et al., 2014, e.g.,).

With a time series 21 years long, it is tempting to investigate whether long term changes in PAR_B can be identified. Fig. 5 shows the percent surface area of the coastal zone of the ~~non polar~~ nonpolar region receiving 2 $\mathrm{mol\ photons\ m^{-2}\ d^{-1}}$ or more. There is a highly significant trend with an increase in percent surface area of 0.1% $\pm$ 0.02 per year ($\pm$ 99% confidence interval). However, separate regression analyses show data shifts occur between the three time periods when the same ocean colour sensors were in operation. The trends are therefore highly variable during specific time periods corresponding to various sets of ocean colour sensors. We conclude that no long-term trend in PAR_B can be identified in this data set.

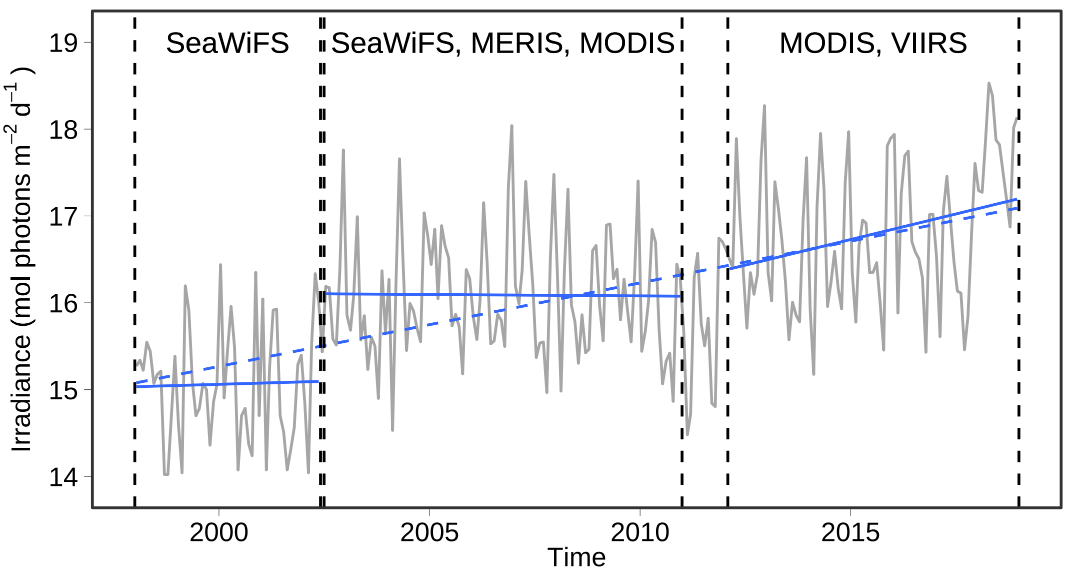

Figure 5. Time series of the surface area (%) of the coastal ~~non polar~~ nonpolar region receiving more than 2 $\mathrm{mol\ photons\ m^{-2}\ d^{-1}}$. The linear regression over 1999-2018 is shown as a dashed line while the result of separate linear regressions for the three time periods with the same set of ocean colour sensors is shown as a solid line.

Table 3. Surface area and average depth of the various pixel classes. Calculations were performed on monthly data sets for the periods indicated. Values reported by Gattuso et al. (2006) are shown in parentheses for comparative purposes. Gattuso et al. (2006) did not report data for the Antarctic. $Z_{1\%}$ is the depth at which benthic irradiance or benthic PAR (PAR_B) equals 1% of surface irradiance or PAR. Available pixels are the pixels for which PAR, K_{PAR}, C_{sat}, and $R_{rs}(555)$ are available for analysis.

	Arctic (June-October)			Nonpolar (January-December)			Antarctic (November-March)		
	Min	Max	Mean	Min	Max	Mean	Min	Max	Mean
Available/Total number of pixels	0.059 (0.20)	0.89 (0.60)	0.51 (0.39)	~~0.110.580.35~~0.62 (0.68)	0.96 (0.90)	0.83 (0.81)	0.11	0.58	0.35
Average depth available pixels (m)	66 (74)	103 (87)	82 (80)	~~148131140~~67 (67)	76 (71)	72 (69)	131	148	140
Average depth missing pixels (m)	67	95	78	~~131138135~~27	81	63	131	138	135
Case 1 pixels/available pixels	0.63 (0.58)	0.86 (0.72)	0.77 0.66)	~~0.320.760.58~~0.62 (0.46)	0.77 (0.65)	0.71 (0.55)	0.32	0.76	0.58
Average depth Case 1 pixels (m)	~~114~~ 80 (86)	~~80~~ 114 (99)	92 (93)	~~157143149~~89 81 (80)	~~81~~ 89 (86)	85 (83)	143	157	149
Case 2 pixels/available pixels	0.14 (0.28)	0.37 (0.42)	0.23 (0.34)	~~0.240.680.42~~0.23 (0.35)	0.38 (0.54)	0.29 (0.45)	0.24	0.68	0.42
Average depth Case 2 pixels (m)	~~64~~ 35 (43)	~~35~~ 64 (70)	46 (55)	~~143107128~~47 31 (44)	~~31~~ 47 (57)	38 (52)	107	143	128
$Z < Z_{1\%}$ pixels/available pixels	0.07	0.21	0.15	~~0.010.070.03~~0.27	0.36	0.31	0.01	0.07	0.03

Table 4. Median values of key variables used by Gattuso et al. (2006) and the present study.

		Gattuso et al. (2006)	Present study
PAR_B (mol photons m^{-2} d^{-1})	Arctic	0.2218	0.0835
	Nonpolar	0.6128	0.2169
Depth (m)	Arctic	31.4	38.5
	Nonpolar	42.5	45
K_{PAR} (m^{-1})	Arctic	0.1407	0.1630
	Nonpolar	0.0968	0.1336
PAR (mol photons m^{-2} d^{-1})	Arctic	19	22
	Nonpolar	41	41

Table 5. Top: Organisms. Surface area (% of the coastal zone) where irradiance does not limit the distribution of photosynthetic organisms. Values reported by Gattuso et al. (2006) are shown in parentheses for comparative purposes. The irradiance thresholds are the first deciles of the minimum light requirements compiled by Gattuso et al. (2006). Data are not reported in the Arctic region for seagrasses and Scleractinian (reef-building) corals where these groups are not present. **Bottom: Communities**. Surface area (% of the coastal zone) where benthic irradiance is higher that the daily community compensation irradiance (NPP>0). The irradiance thresholds are the first deciles of the minimum light requirements compiled by Gattuso et al. (2006). Data are not reported for seagrass communities and coral reefs in the Arctic and Antarctic regions where they do not occur.

	Irradiance	Percent surface area in region			Total surface area
	(mol photons m^{-2} d^{-1})	~~Non polar~~ Arctic	Nonpolar	Antarctic	(10^6 km^2)
Organisms					
Seagrasses	1.3	–	20 (28)	–	~~–~~3.78 (5.27)
Macroalgae					
– Filamentous and slightly corticated filamentous	0.2	~~37 (42)~~18 (26)	37 (42)	4	8.21 (9.50)
– Corticated foliose, corticated and foliose	0.098	~~43 (47)~~23 (30)	43 (47)	5	9.65 (10.68)
– Leathery and articulated calcareous	0.040	~~50 (54)~~29 (36)	50 (54)	6	11.28 (12.37)
– Crustose	0.001	~~70 (66)~~49 (51)	70 (66)	19	16.32 (15.55)
Microphytobenthos	0.4	~~31 (37)~~14 (22)	31 (37)	3	6.73 (8.31)
Scleractinian corals	0.18	–	38 (43)	–	~~–~~7.29 (8.09)
Communities					
Seagrass beds	2.4	–	15 (23)	–	~~–~~2.78 (4.32)
Macroalgal communities	1.6	~~18 (26)~~ 8 (13)	18 (26)	2	3.91 (5.71)
Microphytobenthic communities	0.24	~~36 (41)~~ 17 (25)	36 (41)	3	7.83 (9.19)
Coral reefs	4.4	–	10 (19)	–	–

4 Data availability

1. **The geographical and optical data** generated and used in this paper are openly available at the World Data Center PANGAEA: Gentili and Gattuso (2020); https://doi.pangaea.de/10.1594/PANGAEA.910898. It consists of 14 netCDF files with an unique dimension (the coastal pixel number) which is identical for all files.

   – a netCDF file with geographical information (latitude, longitude, depth, area of the pixels) (CoastalLight_geo.nc; about 1.2 Gb)

   – a netCDF file with the climatology over the whole 21 year period calculated as the mean values of the ~~242~~ monthly data of PAR, K_{PAR} and PAR_B (CoastalLight_00.nc; about 1.1 Gb)

   – 12 netCDF ~~file with monthly~~ files with monthly climatologies (mean of the ~~21 monthly~~ values of PAR, K_{PAR} and PAR_B):

     - Monthly climatology, January: CoastalLight_01.nc (6.2 Gb)
     - Monthly climatology, February: CoastalLight_02.nc (6.8 Gb)
     - Monthly climatology, March: CoastalLight_03.nc (7 Gb)
     - Monthly climatology, April: CoastalLight_04.nc (7 Gb)
     - Monthly climatology, May: CoastalLight_05.nc (7 Gb)
     - Monthly climatology, June: CoastalLight_06.nc (9.6 Gb)
     - Monthly climatology, July: CoastalLight_07.nc (10.6 Gb)
     - Monthly climatology, August: CoastalLight_08.nc (11 Gb)
     - Monthly climatology, September: CoastalLight_09.nc (10.4 Gb)
     - Monthly climatology, October: CoastalLight_10.nc (7.8 Gb)
     - Monthly climatology, November: CoastalLight_11.nc (6.4 Gb)
     - Monthly climatology, December: CoastalLight_12.nc (6 Gb)

2. **The surface area of three regions** (Arctic, Antarctic and ~~non-polar~~nonpolar) receiving an irradiance above a certain threshold is available using the R package *CoastalLight*: https://github.com/jpgattuso/CoastalLight. To install the package, proceed as follows:

   – install.packages("devtools")

   – library(devtools)

   – install_github("jpgattuso/CoastalLight")

   – use function *cl_surface* of the *CoastalLight* package

3. **The surface area of a subregion** of one of the regions above receiving an irradiance above a certain threshold can be derived by (complete information can be found in the documentation of the *CoastalLight* package):

   – connecting to the web server http://obs-vlfr.fr/Pfunction to calculate and download its $\mathcal{P}$-function

   – then using this $\mathcal{P}$-function with function *cl_surface* of the *CoastalLight* package.

5 Conclusions

This study builds on the first, and still only, global distribution of photosynthetically available radiations reaching the sea floor (Gattuso et al., 2006). It improves the geographical and depth resolutions, and covers a much longer period of time. Despite these key improvements, several limitations inherent to the approach remain. While the spatial resolution is twice better than the previous products, 4.6 km at the equator it is still coarse for investigating the distribution and function of organisms and communities which change at much finer scales. The parameterization used to convert reflectance data to irradiance is approximate in Case 2 waters. Finally, light absorption in the benthic nepheloid layer is not taken into consideration. The global distribution of PAR_B we provide is derived with state-of-the-art data and computations and is arguably the best that can be offered at this time. Despite its shortcomings, it should considerably improve estimates of the geographical and depth distributions of photosynthetic organisms and ecosystems and help assess their contribution to global biogeochemical cycles.

Appendix A: Graphical representation of P-functions

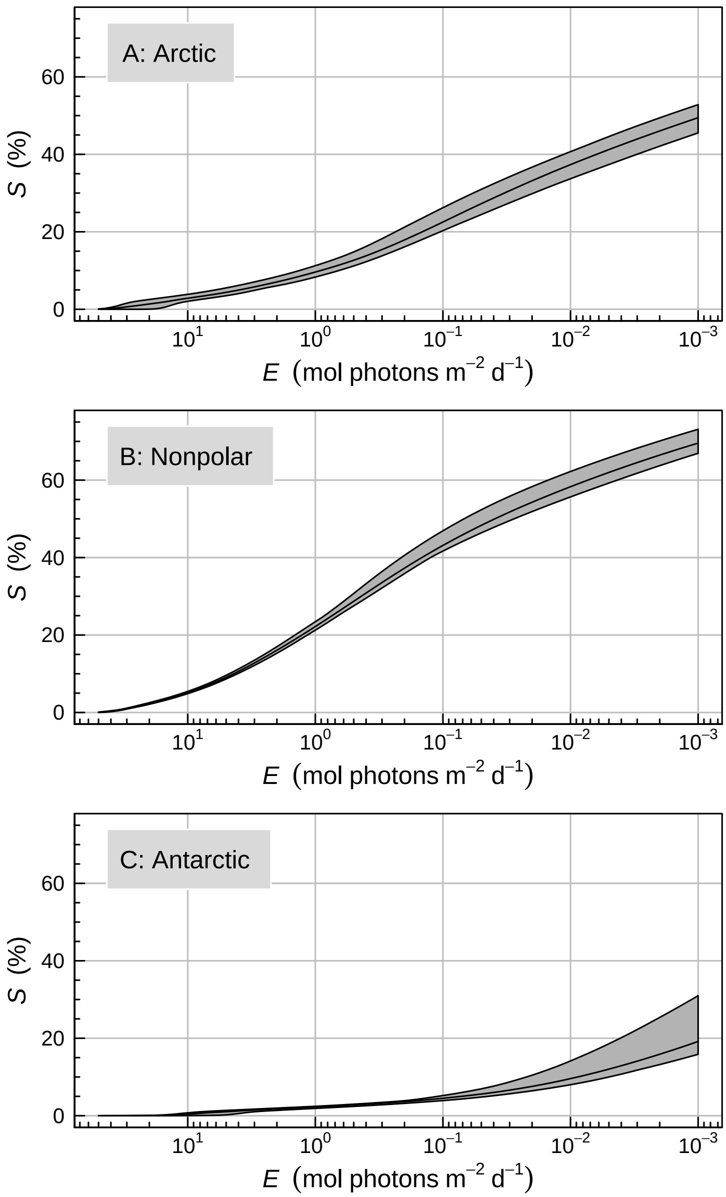

Figure A1. Cumulative surface area of the sea floor (~~S~~S) receiving irradiance above a prescribed threshold (~~E_z~~E). Data are expressed in percent of the total surface area of each region ($19,080,010$, $6,100,532$ and $146,171$ km^2, respectively for the ~~non-polar~~nonpolar, Arctic and Antarctic regions). The shaded ~~area shows~~ areas show the monthly variability.

Author contributions. J.-P.G conceptualized the study. B.G. developed the methods, processed the data, and carried out all data analyses, including software development, with periodic feedback from J.-P.G. J.-P.G wrote the original draft with contributions from B.G., D.A. and D.D. All authors reviewed and edited the final manuscript.

Competing interests. None.

Acknowledgements. This is paper a product of The Ocean Solutions Initiative (http://bit.ly/2xJ3EV6), with support from Prince Albert II of Monaco Foundation, Veolia Foundation, IAEA Ocean Acidification International Coordination Centre and French Facility for Global Environment; and of the EU-H2020 project INTAROS (grant #727890). This paper is a contribution to an Euromarine project (http://euromarinenetwork.eu/activities/role-macroalgae-global-ocean-carbon-budget) led by Dorte Krause-Jensen. Participants of the foresight workshop held in Granada in 2019, especially Jorge Assis, Carlos Duarte and Dorte Krause-Jensen are gratefully acknowledged for stimulating discussions.

References

ACRI-ST GlobColour Team: GLOBCOLOUR Product User Guide Version 4.1, ACRI-ST, 2017.

Antoine, D., André, J.-M., and Morel, A.: Oceanic primary production. 2. Estimation at global sclae from satellite (coastal zone color scanner) chlorophyll, Glob. Biogeochem. Cycles, 10, 43–55, 1996.

Assis, J., Tyberghein, L., Bosch, S., Verbruggen, H., Serrão, E. A., and Clerck, O. D.: Bio-ORACLE v2.0: Extending marine data layers for bioclimatic modelling, Glob. Ecol. Biogeogr., 27, 277–284, 2018.

Attard, K., Hancke, K., Sejr, M., and Glud, R.: Benthic primary production and mineralization in a High Arctic fjord: in situ assessments by aquatic eddy covariance, Mar. Ecol. Prog. Ser., 554, 35–50, 2016.

Claustre, H. and Maritorena, S.: The many shades of ocean blue, Science, 302, 1514–1515, 2003.

Delesalle, B., Pichon, M., Frankignoulle, M., and Gattuso, J.-P.: Effects of a cyclone on coral reef phytoplankton biomass, primary production and composition (Moorea island, French Polynesia), J. Plankt. Res., 15, 1413–1423, 1993.

Doxaran, D., Devred, E., and Babin, M.: A 50terrestrial particles delivered by the Mackenzie River into the Beaufort Sea (Canadian Arctic Ocean) over the last 10 years, Biogeosciences, 12, 3551–3565, 2015.

Duarte, C. M.: Reviews and syntheses: Hidden forests, the role of vegetated coastal habitats in the ocean carbon budget, Biogeosciences, 14, 301–310, 2017.

Eriander, L.: Light requirements for successful restoration of eelgrass (Zostera marina L.) in a high latitude environment - Acclimatization, growth and carbohydrate storage, J. Exp. Mar. Biol. Ecol., 496, 37–48, 2017.

Eyre, B. D., Santos, I. R., and Maher, D. T.: Seasonal, daily and diel N2 effluxes in permeable carbonate sediments, Biogeosciences, 10, 2601–2615, 2013.

Feng, L., Hu, C., Chen, X., and Song, Q.: Influence of the Three Gorges Dam on total suspended matters in the Yangtze Estuary and its adjacent coastal waters: Observations from MODIS, Remote Sens. Environ., 140, 779–788, 2014.

Filbee-Dexter, K. and Scheibling, R. E.: Detrital kelp subsidy supports high reproductive condition of deep-living sea urchins in a sedimentary basin, Aquatic Biology, 23, 71–86, 2015.

Garver, S. A. and Siegel, D. A.: Inherent optical property inversion of ocean color spectra and its biogeochemical interpretation: 1. Time series from the Sargasso Sea, J. Geophys. Res.: Oceans, 102, 18 607–18 625, 1997.

Gattuso, J.-P., Gentili, B., Duarte, C., Kleypas, J., Middelburg, J., and Antoine, D.: Light availability in the coastal ocean: impact on the distribution of benthic photosynthetic organisms and their contribution to primary production, Biogeosciences, 3, 489–513, 2006.

Gentili, B. and Gattuso, J.-P.: Photosynthetically available radiation (PAR) on the seafloor calculated from 21 years of ocean colour satellite data, PANGAEA, p. doi:10.1594/PANGAEA.910898, 2020.

Glud, R., Woelfel, J., Karsten, U., Kühl, M., and Rysgaard, S.: Benthic microalgal production in the Arctic: applied methods and status of the of the current database, Bot. Mar., 52, 559–571, 2009.

He, X., Pan, D., Bai, Y., Wang, T., Chen, C.-T. A., Zhu, Q., Hao, Z., and Gong, F.: Recent changes of global ocean transparency observed by SeaWiFS, Cont. Shelf Res., 143, 159–166, 2017.

Krause-Jensen, D. and Duarte, C. M.: Substantial role of macroalgae in marine carbon sequestration, Nat. Geosci., 9, 737–742, 2016.

Krause-Jensen, D., Lavery, P., Serrano, O., Marbà, N., Masque, P., and Duarte, C.: Sequestration of macroalgal carbon: the elephant in the Blue Carbon room, Biol. Lett., 14, 20180 236, 2018.

Lee, Z., Shang, S., Hu, C., Du, K., Weidemann, A., Hou, W., Lin, J., and Lin, G.: Secchi disk depth: A new theory and mechanistic model for underwater visibility, Remote Sens. Environ., 169, 139–149, 2015.

Loisel, H., Mangin, A., Vantrepotte, V., Dessailly, D., Dinh, D., Garnesson, P., Ouillon, S., Lefebvre, J.-P., Mériaux, X., and Phan, T.: Variability of suspended particulate matter concentration in coastal waters under the Mekong's influence from ocean color (MERIS) remote sensing over the last decade, Remote Sens. Environ., 150, 218–230, 2014.

Macreadie, P.: The future of Blue Carbon science, Nat. Comm., 2019.

Maritorena, S., Siegel, D., and Peterson, A.: Optimization of a semianalytical ocean color model for global-scale applications, Appl. Opt., 41, 2705–2714, 2002.

Maritorena, S., d'Andon, O. H. F., Mangin, A., and Siegel, D. A.: Merged satellite ocean color data products using a bio-optical model: Characteristics, benefits and issues, Remote Sens. Environ., 114, 1791–1804, 2010.

Morel, A. and Bélanger, S.: Improved detection of turbid waters from ocean color sensors information, Remote Sens. Environ., 102, 237–249, 2006.

Morel, A. and Gentili, B.: Diffuse reflectance of oceanic waters.3. Implication of bidirectionality for the remote-sensing problem, Appl. Opt., 35, 4850–4862, 1996.

Morel, A., Huot, Y., Gentili, B., Werdell, P., Hooker, S., and Franz, B.: Examining the consistency of products derived from various ocean color sensors in open ocean (Case 1) waters in the perspective of a multi-sensor approach, Remote Sens. Environ., 111, 69–88, 2007.

Tyler, J.: The Secchi disk, Limnol. Oceanogr., 13, 1–6, 1968.

Weinberg, S.: Submarine daylight and ecology, Mar. Biol., 37, 291–304, 1976.

Wessel, P., Smith, W., Scharroo, R., Luis, J., and Wobbe, F.: Generic Mapping Tools: improved version released, Eos, Transactions American Geophysical Union, 94, 409–410, 2013.